

Fe-based high temperature superconductivity with $T_c=31\text{K}$ bordering an insulating antiferromagnet in $(\text{Tl,K})\text{Fe}_x\text{Se}_2$ Crystals

Minghu Fang^{1*}, Hangdong Wang^{1,2}, Chiheng Dong¹,
Zujuan Li¹, Chunmu Feng¹, Jian Chen¹, H.Q. Yuan¹

¹ Department of Physics, Zhejiang University, Hangzhou 310027, China

² Department of Physics, Hangzhou Normal University, Hangzhou 310036, China

Up to now, there have been two material families, the cuprates¹ and the iron-based compounds²⁻¹² with high-temperature superconductivity (HTSC). An essential open question is whether the two classes of materials share the same essential physics. In both, superconductivity (SC) emerges when an antiferromagnetic (AFM) ordered phase is suppressed. However, in cuprates, the repulsive interaction among the electrons is so strong that the parent compounds are “Mott insulators.” By contrast, all iron-based parents are metallic. One perspective¹³⁻¹⁴ is that the iron-based parents are weakly correlated and that the AFM arises from a strong “nesting” of the Fermi surfaces. An alternative¹⁵⁻¹⁸ view is that the electronic correlations in the parents are still sufficiently strong to place the system close to the boundary between itinerancy and electronic localization. A key strategy to differentiate these views is to explore whether the iron-based system can be tuned into a Mott insulator. Here we identify an insulating AFM in $(\text{Tl,K})\text{Fe}_x\text{Se}_2$ by introducing Fe-vacancies and creating superconductivity in the Fe-planar. With the increasing Fe-content, the AFM order is reduced. When the magnetism is eliminated, a superconducting phase with T_c as high as 31K (and a T_c^{onset} as high as 40K) is induced. Our findings indicate that the correlation effect plays a crucial role in the iron-based superconductors. $(\text{Tl,K})\text{Fe}_x\text{Se}_2$, therefore, represents the first Fe-based high temperature superconductor near an insulating AFM.

All the iron-based superconductors share a common layered structure based on a square planar Fe^{2+} layer [see Fig. 1h], tetrahedrally coordinated pnictogen¹⁹⁻²¹ (P, As) or chalcogen²² (S, Se, Te) anions. It is now widely thought that the interaction that leads to the HTSC originates within these common Fe^{2+} layers, similar in nature to the common CuO_2 layer in the cuprate HTSCs. The crystal structure²² of stoichiometric TlFe_2Se_2 , which is shown in Fig. 1a, is the same as that of the BaFe_2As_2 (122-type iron-pnictide) with the ThCr_2Si_2 -type. But in the TlFe_2Se_2 compound, one of the known two 122-type iron-chalcogenide, another TlFe_2S_2 ²³, Tl occurring as a monovalent Tl^{+1} here, there are always Fe vacancies on the Fe square planar^{24,25}. So the actual component should be rewritten as TlFe_xSe_2 ($1.3 \leq x < 2.0$). The most interesting is that Fe square layers in TlFe_xSe_2 and TlFe_xS_2 compounds also exhibit a long-range AFM order. Based on the Mössbauer and neutron diffraction studies, Haggstrom et al.²⁶ and Sabrowsky et al.²⁷ argued that the AFM order in TlFe_xSe_2 and TlFe_xS_2 compounds is associated with the long range order of Fe-vacancy, as shown in Fig. 1 (f) and (g) for $x=1.5$ and 1.6 , respectively. In this opinion, the AFM order might be suppressed by increasing the Fe content, in addition, the Fe layer should become a square pattern ($x=2.0$) in the end (Fig. 1h), which exists in all the Fe-based superconductors. The suspecting for superconductivity emergence in this new 122-type iron-chalcogenide motivates us to grow TlFe_xSe_2 single crystals with a relatively high Fe-content.

At first, we tried to grow TlFe_xSe_2 single crystals with a relatively large x value using various nominal compositions as the starting materials, *i.e.* $\text{Tl}_z\text{Fe}_2\text{Se}_2$ ($0.4 \leq z \leq 1.0$), TlFe_zSe_2 ($1.5 \leq z \leq 3$). We have gotten a series of TlFe_xSe_2 ($1.3 \leq x \leq 1.70$) single crystals. We observed an AFM transition at the Neel temperature $T_N=365\text{K}$ and 265K , respectively, in the $\text{TlFe}_{1.30}\text{Se}_2$ and $\text{TlFe}_{1.47}\text{Se}_2$ crystals. Particularly, we found that the temperature dependence of magnetic susceptibility, $\chi(T)$, shows a similar behavior to that in all the parent of the Fe-based compounds²⁸⁻³³ (see Fig. S1a and S1b). And we also observed that their temperature dependence of *ab*-plane

resistivity, $\rho(T)$, exhibits a thermally activated behavior with a activation energy E_a of 80.2meV and 57.7meV (see the inset in Fig. S1a and S1b), respectively. Furthermore, superconductivity with a transition temperature 22.4K (T_c^{mid} , the middle temperature of the transition) and zero resistivity at 20K (T_c^{zero} , the temperature zero resistance) is indeed first observed in the $\text{TlFe}_{1.70}\text{Se}_2$ crystals (See Fig. S2), but magnetic susceptibility measurement shows its superconducting volume fraction (SVF) being very small (<3%). At the same time, we found that it is difficult to grow a TlFe_xSe_2 single crystal with $x>1.7$.

This indicates that, in order to get bulk superconductivity in this system, it is necessary to increase further the Fe-content. We tried to grow $(\text{Tl,K})\text{Fe}_x\text{Se}_2$ single crystals by adding K in the starting materials and choosing three group nominal compositions as the starting materials, *i.e.* $\text{Tl}_{0.5}\text{K}_z\text{Fe}_2\text{Se}_2$ ($0.15\leq z\leq 0.45$), $\text{Tl}_{0.4}\text{K}_z\text{Fe}_2\text{Se}_2$ ($0.2\leq z\leq 0.5$) and $\text{Tl}_{0.8-z}\text{K}_z\text{Fe}_2\text{Se}_2$ ($0.1\leq z\leq 0.4$). Based on the composition analyses (see Table S1) for the grown crystals by an Energy Dispersive X-ray Spectrometer (EDXS), we indeed found that the addition of K element can lead to the increase of the Fe content in the grown crystals, the maximum x value can reach to 1.88 (see Table S1). Figure S3 in the Supplementary shows the Fe and K content in the grown crystals as a function of the K content in the starting materials with the nominal composition $\text{Tl}_{0.5}\text{K}_z\text{Fe}_2\text{Se}_2$ ($0.15\leq z\leq 0.45$). And we also found that the composition of Tl+K in the grown crystals is always of 1.0, regardless of their composition in the starting materials, although the relative ratio between Tl and K depends on the starting composition. A series of $\text{Tl}_{1-y}\text{K}_y\text{Fe}_x\text{Se}_2$ ($1.50\leq x\leq 1.88$, $0.14\leq y\leq 0.57$) single crystals has been gotten. Figure 1b presents the photos of $\text{Tl}_{0.48}\text{K}_{0.52}\text{Fe}_{1.50}\text{Se}_2$ crystals before cleaved and one piece crystal of $\text{Tl}_{0.64}\text{K}_{0.36}\text{Fe}_{1.83}\text{Se}_2$.

Figure 1c, 1d and 1e show the single crystal and powder x-ray diffraction (XRD) patterns for the $\text{Tl}_{0.64}\text{K}_{0.36}\text{Fe}_{1.83}\text{Se}_2$ and $\text{Tl}_{0.48}\text{K}_{0.52}\text{Fe}_{1.50}\text{Se}_2$. All the peaks in the powder XRD pattern can be well indexed with a ThCr_2Si_2 -type structure (space

group: $I4/mmm$). The lattice parameters, $a=3.88\text{\AA}$, $c=14.05\text{\AA}$ for $\text{Tl}_{0.64}\text{K}_{0.36}\text{Fe}_{1.83}\text{Se}_2$; $a=3.90\text{\AA}$, $c=13.99\text{\AA}$ for $\text{Tl}_{0.48}\text{K}_{0.52}\text{Fe}_{1.50}\text{Se}_2$ crystals were obtained by the fitting XRD data. Broader peaks in the powder XRD patterns might indicate the existence of some disorder in the crystals, and it is difficult to observe super-lattice peaks of Fe vacancy order. Only $(00l)$ peaks were observed in the single crystal XRD patterns, indicating that the crystallographic c axis is perpendicular to the plane of the single crystal. The single crystal and powder XRD results for other composition samples are similar to these, their lattice parameters are listed in Table S1 in the Supplementary.

Figure 2a and 2b shows the $\rho(T)$ for the $(\text{Tl,K})\text{Fe}_x\text{Se}_2$ ($1.50 \leq x \leq 1.85$) crystals. For the $x=1.50$ and 1.65 crystals, their resistivity increases rapidly with decreasing temperature and the room temperature resistivity are about $27.8 \text{ m}\Omega\cdot\text{cm}$ and $27.2 \text{ m}\Omega\cdot\text{cm}$, respectively. Similar to the case of the $\text{TlFe}_{1.30}\text{Se}_2$ and $\text{TlFe}_{1.47}\text{Se}_2$ crystals mentioned above, their $\rho(T)$ also exhibits the thermally activated behavior: $\rho = \rho_0 \exp(E_a/k_B T)$, where ρ_0 and k_B are a prefactor and the Boltzmann constant, respectively. The activation energy E_a was estimated to be about 36 meV and 24 meV from the fitting results (see red line for $x=1.50$ crystal in Fig 2c, in Fig. S1c for $x=1.64$ crystal), respectively.

The most surprising is that the $\chi(T)$ behavior for the $x=1.50$, and 1.65 insulators, as well as the $\text{TlFe}_{1.30}\text{Se}_2$ and $\text{TlFe}_{1.47}\text{Se}_2$ mentioned above (see Fig S1a and S1b), is very similar to that²⁹ in the BaFe_2As_2 , which is a parent of 122-type iron-pnictide and a metal. As shown in the inset in Fig. 2c, the susceptibility of the $x=1.50$ crystal decreases monotonically with temperature and shows a linear temperature dependence above 250K . At 250K the susceptibility shows a rapid decrease which may be ascribed to the occurrence of AFM transition associated with the Fe-vacancy order shown in Fig. 1(f). In addition, the susceptibility at 400K is $3.48 \times 10^{-3} \text{ emu/mol}$, which is the same order of magnitude as that of BaFe_2As_2 ²⁹. For the $x=1.64$ crystal, the susceptibility shows a rapid decrease at 123K , which

may be associated with the Fe-vacancy order shown in Fig. 1(g), and high temperature susceptibility exhibits a similar behavior to that of the $x=1.50$ crystal. These results indicate that the T_N decreases with the increase of the Fe content in the crystal. The observed increase of χ with T in the FeAs-based compounds has been attributed to itinerant electron antiferromagnetic spin fluctuation³², or the alternatively to AF correlations between local moments in a strong coupling description³⁴, as discussed for the cuprate parent compounds³⁵. Here, our findings support obviously the latter, because the $(\text{Tl,K})\text{Fe}_x\text{Se}_2$ ($x=1.30, 1.47, 1.50$ and 1.64) crystals with a super-lattice of Fe-vacancy are an insulator. Recently, Zhu et al³⁶. pointed out by means of theory calculations that the expansion of the Fe square lattice can give rise to a narrowing of the 3d-bands and a concomitant enhancement of U/t (Here t and U are respectively the characteristic band-width and Coulomb repulsion of the Fe 3d electrons.) pushes the system to the Mott region.

With the x value further increasing, the ρ value at the lower temperatures rapidly decreases, for example, at 40K, the $x=1.64$ crystal $\rho=18.6 \Omega\cdot\text{cm}$, while the $x=1.69$ crystal ρ drops to $0.46 \Omega\cdot\text{cm}$. The interesting is that a superconducting transition starts to occur at 25.8K and 27.6K, respectively, for $x=1.69$ and 1.76 crystal, but no zero resistivity is observed above 2K (see Fig. 2a), indicating that superconductivity starts to emerge and coexists with an insulator phase in the $1.69 \leq x \leq 1.76$ crystals. In the $x=1.78$ crystal, a sharp superconducting transition occurs at $T_c^{\text{mid}}=28.4\text{K}$, and reach to zero resistivity at $T_c^{\text{zero}}=27.4\text{K}$, confirmed by the existence of diamagnetism below T_c (See Fig. 2d). For the $x=1.83$, *i.e.* $\text{Tl}_{0.64}\text{K}_{0.36}\text{Fe}_{1.83}\text{Se}_2$ crystal, T_c^{mid} increases to 31.1K and $T_c^{\text{zero}}=30\text{K}$. And for the $x=1.84$ ($\text{Tl}_{0.69}\text{K}_{0.31}\text{Fe}_{1.84}\text{Se}_2$) and 1.85 ($\text{Tl}_{0.75}\text{K}_{0.25}\text{Fe}_{1.85}\text{Se}_2$) crystals, although their T_c^{mid} values are almost the same as that in $x=1.83$, they have a much larger SVF (see Fig.2d). We found that the superconducting transition temperatures, T_c^{mid} and T_c^{zero} , vary only with the Fe content in the crystals, and are independent of the K content in the crystals.

In addition, for both the $x=1.78$ and 1.83 crystals, their ρ value has a maximum

at about 75K, where a metal-insulator transition occurs. While for the $x=1.85$ crystal, although it exhibits a bulk superconductivity below 30K with larger SVF, its resistivity at the normal state is almost independent of T and about of 10 m Ω cm. Hall coefficient measurements have confirmed that they are an electron type superconductor (see Fig.4), and the carrier concentration in $x=1.83$ and 1.85 crystals is almost the same, although there is some differences in $\rho(T)$ at the normal state between them. This implies that $(\text{Tl,K})\text{Fe}_x\text{Se}_2$ ($1.78 \leq x \leq 1.85$) might reside in the under-doping region in the phase diagram. There is a tendency that T_c should increase to the highest one in the crystal with an optimal Fe-content.

We check again the superconducting transition in $\rho(T)$ for the $(\text{Tl,K})\text{Fe}_x\text{Se}_2$ crystals with different x value. As shown in Fig. 3a, for the $x=1.78$ crystal, there is only a sharp transition at $T_c=28.4\text{K}$. While in the $x=1.84$ crystal, two transitions occur at $T_c=29.8\text{K}$ and 33.0K , respectively. Most interesting is that three transitions occur at $T_c=30.4$, 34.1 , and 40.4K , respectively, in the $\text{Tl}_{0.75}\text{K}_{0.25}\text{Fe}_{1.88}\text{Se}_2$ crystal, which is one with the highest Fe content gotten by us. The existence of superconducting phase with $T_c=40\text{K}$ in the crystals with higher Fe content is also confirmed by $\rho(T)$ at various fields for the $\text{Tl}_{0.64}\text{K}_{0.36}\text{Fe}_{1.83}\text{Se}_2$ crystal, as shown in Fig. 3d. Compared with the $x=1.78$ crystal with only one transition at 28.4K , the transition at each magnetic field starts at 40K for the $x=1.83$ crystal. The multi-transition in $\rho(T)$ was observed in all the crystals with $x \geq 1.83$, regardless of the K content. This means that the domains with various Fe content, corresponding to different carrier concentration, perhaps exist in the crystals. In the majority domain, superconductivity with $T_c=30\text{K}$ emerges. The volume fraction of the domains with higher T_c value and higher Fe content, which should be unstable due to the Fe^{2+} valence limitation, may be very small because no diamagnetic signal appears at higher temperature. To our knowledge, this phase separation behavior is first observed in Fe-based superconductors. Superconductivity with $T_c=40\text{K}$ emergence in the $(\text{Tl,K})\text{Fe}_x\text{Se}_2$ crystals with relatively high Fe content is reminiscent of the highest $T_c=38\text{K}$ in the optimal doping $\text{Ba}_{1-x}\text{K}_x\text{Fe}_2\text{As}_2$ compound⁸.

Bulk superconductivity with $T_c=40\text{K}$ may emerge in the crystal with an optimal Fe-content, but it is difficult to realize in this system due to the Fe^{2+} valence limitation.

In order to explore the effect of the Fe content on the electronic structure in $(\text{Tl,K})\text{Fe}_x\text{Se}_2$ system, we choose four crystals with $x=1.84, 1.83, 1.64$ and 1.50 to measure Hall coefficient. Their temperature dependence of Hall coefficient, $R_H(T)$, is shown in Fig. 4. The negative value of R_H in all the temperature range indicates that the carrier in $(\text{Tl,K})\text{Fe}_{2-x}\text{Se}_2$ compound is dominated by electrons, which is consistent with the electronic band calculation result for the stoichiometric TlFe_2Se_2 reported by Zhang et al.³⁷ For both the $\text{Tl}_{0.48}\text{K}_{0.52}\text{Fe}_{1.50}\text{Se}_2$ and $\text{Tl}_{0.53}\text{K}_{0.47}\text{Fe}_{1.64}\text{Se}_2$ crystals, which are an AFM insulator, the $|R_H|$ value increases sharply at $T_N=250$ and 123K , respectively, where an electron localization occurs. This is a typical behavior of the AFM Mott insulator. The increase of the Fe-content results in the enhancement of the carrier concentration ($|R_H|$ value decrease), which can be regarded as a self-doping of Fe^{2+} electron to the Fe layer with a super-lattice of Fe vacancy.

We have constructed a phase diagram of the magnetism and superconductivity for $(\text{Tl,K})\text{Fe}_x\text{Se}_2$ with $1.3 \leq x \leq 2.0$, which is shown in Fig. 5. There are three composition regions with distinct physical properties. For the region of $1.3 \leq x < 1.7$, the compound is an AFM insulator, which may be associated with the existence of various super-lattice of Fe-vacancy. The Néel temperature, T_N , decreases with increasing Fe content. In the region of $1.70 \leq x < 1.78$, a superconducting transition was observed in $\rho(T)$, but superconducting volume fraction is less than 1% estimated from the susceptibility data. An inhomogeneity of Fe-vacancy distribution may result in the coexistence of superconductivity and insulator phase. In the region of $1.78 \leq x \leq 1.88$, bulk superconductivity emerges. The observation of multi-transition in $\rho(T)$ for the crystals with $x \geq 1.83$ implies that phase separation may occur in the crystals and an optimal Fe content for bulk superconductivity with

the highest $T_c=40\text{K}$ does not reach due to the limitation of Fe valence. Correspondingly, the phase diagram of $(\text{Tl,K})\text{Fe}_x\text{Se}_2$ system appears very similar to that of the cuprate superconductors.

In summary, we first report the measurements of resistivity, magnetic susceptibility and Hall coefficient for $(\text{Tl,K})\text{Fe}_x\text{Se}_2$ crystals. We found that $(\text{Tl,K})\text{Fe}_x\text{Se}_2$ ($1.3 \leq x < 1.7$) crystals are antiferromagnetic insulators. With the increase of the Fe content, bulk superconductivity with $T_c^{\text{mid}}=31\text{K}$ occurs in $(\text{Tl,K})\text{Fe}_x\text{Se}_2$ ($1.78 \leq x \leq 1.88$) crystals, and the onset superconducting transition temperature T_c^{onset} goes up as high as 40K. It is found that the phase diagram of $(\text{Tl,K})\text{Fe}_x\text{Se}_2$ system is very similar to that of the cuprate superconductors. The evolution from an AFM insulating state to a superconducting state can be driven by increasing Fe content in $(\text{Tl,K})\text{Fe}_x\text{Se}_2$, making these compounds a promising new platform for further exploration of the electron correlation effect. At the same time, our results show that orderly introducing Fe vacancy represents a means to induce Fe-based parents to the Mott insulating part of the phase diagram.

Method Summary

$(\text{Tl,K})\text{Fe}_x\text{Se}_2$ single crystals were grown using a self-flux method. The starting materials Tl_2Se , K_2Se , Fe and Se powder were mixed according to a various nominal composition in a glove box and loaded in a thin corundum crucible. Then the crucible was sealed in an evacuated quartz tube. The sealed silica tube was slowly heated to 950°C and held for 6 hours. Then let temperature decrease to 700°C in a rate of $3^\circ\text{C}/\text{hrs}$, and finally cool down to room temperature by switching off the furnace. In each step to prepare sample, it is very important to manage carefully due to Tl_2Se poison. The composition of crystals was determined using an Energy Dispersive X-ray Spectrometer (EDXS). The electrical resistivity and Hall coefficient were measured on a Physical Properties Measurement System (PPMS; Quantum Design). The dc magnetic susceptibility was measured by using SQUID (Quantum Design).

Reference:

1. Bednorz, J. G. & Muller, K. A. Possible High-Tc Superconductivity in the Ba-La-Cu-O System. *Zeit. Fur Physik B-Condensed Matter* **64**, 189-193 (1986)
2. Kamihara, Y., Watanabe, T., Hirano, M. & Hosono, H. Iron-based layered superconductor La[O_{1-x}F_x]FeAs (x=0.05-0.12) with T_c=26 K. *J. Am. Chem. Soc.* **130**, 3296-3297 (2008).
3. Chen, X. H. *et al.* Superconductivity at 43K in SmFeAsO_{1-x}F_x. *Nature* **453**, 761-762(2008)
4. Chen, G. F. *et al.* Superconductivity at 41K and its competition with spin-density-wave instability in layered CeO_{1-x}F_xFeAs. *Phys. Rev. Lett.* **100**, 247002(2008)
5. Ren, Z. A. *et al.* Superconductivity in the iron-based F-doped layered quaternary compound Nd[O_{1-x}F_x]FeAs. *Europhys. Lett.* **82**, 57002(2008)
6. Wen, H.H., *et al.* Superconductivity at 25K in hole-doped (La_{1-x}Sr_x)OFeAs. *Europhys. Lett.* **82**, 17009(2008)
7. Wang, C. *et al.* Thorium-doping induced superconductivity up to 56K in Gd_{1-x}Th_xFeAsO. *Europhys. Lett.* **83**, 67006(2008)
8. Rotter, M., Tegel, M., and Johrendt, D. Superconductivity at 38K in the iron arsenide (Ba_{1-x}K_x)Fe₂As₂. *Phys. Rev. Lett.* **101**, 107006(2008)
9. Sefat, A.S., *et al.* Superconductivity at 22K in Co-doped BaFe₂As₂ crystals. *Phys. Rev. Lett.* **101**, 117004(2008)
10. Wang, X. C. *et al.* The superconductivity at 18 K in LiFeAs system. *Solid State Commun.* **148**, 538-540, doi:DOI 10.1016/j.ssc.2008.09.057 (2008).
11. Hsu, F. C. *et al.* Superconductivity in the PbO-type structure alpha-FeSe. *Proc. Nat. Acad. Sci.* **105**, 14262-14264, (2008).
12. Fang, M. H. *et al.* Superconductivity close to magnetic instability in Fe(Se_{1-x}Te_x). *Physical Review B* **78**, 224503 (2008).
13. Mazin, I. I., Singh, D. J., Johannes, M. D. & Du, M. H. Unconventional Superconductivity with a Sign Reversal in the Order Parameter of LaFeAsO_{1-x}F_x. *Phys. Rev. Lett.* **101**, 057003 (2008).

14. Yang, W. L. *et al.* Evidence for weak electronic correlations in iron pnictides. *Phys. Rev. B* **80**, 014508 (2009)
15. Si, Q. & Abrahams, E. Strong Correlations and Magnetic Frustration in the High T_c Iron Pnictides. *Phys. Rev. Lett.* **101**, 076401 (2008)
16. Dai, J. H., Si, Q. M., Zhu, J. X. & Abrahams, E. Iron pnictides as a new setting for quantum criticality. *Proc. Nat. Acad. Sci.* **106**, 4118-4121 (2009).
17. Seo, K., Bernevig, B. A. & Hu, J. Pairing Symmetry in a Two-Orbital Exchange Coupling Model of Oxypnictides. *Phys. Rev. Lett.* **101**, 206404 (2008)
18. Ma, F., Lu, Z.-Y. & Xiang, T. Arsenic-bridged antiferromagnetic superexchange interactions in LaFeAsO. *Phys. Rev. B* **78**, 224517 (2008)
19. de la Cruz, C *et al.* Magnetic order close to superconductivity in the iron-based layered LaO_{1-x}F_xFeAs system. *Nature* **453**, 899-902(2008)
20. Huang, Q. *et al.* Neutron-diffraction measurements of magnetic order and a structural transition in the parent BaFe₂As₂ compound of FeAs-based high-temperature superconductors, *Phys. Rev. Lett.* **101**, 257003 (2008)
21. Takahashi, H. *et al.* Superconductivity at 43 K in an iron-based layered compound LaO_{1-x}F_xFeAs. *Nature* **453**, 376-378 (2008)
22. Bao, W. *et al.* Tunable $(\delta\pi, \delta\pi)$ -type antiferromagnetic order in α -Fe(Te,Se) superconductors. *Phys. Rev. Lett.* **102**, 247001 (2009)
23. Klepp, K. and Boller, H. Ternäre Thallium-Übergangsmetall-Chalkogenide mit ThCr₂Si₂-Struktur. *Monatsh. Chem.* **109**, 1049-1057(1978)
24. Zabel, M. & Range, K. J. Structure and Phase-Changes of Tl₂Fe₃S₄. *Rev. Chim. Miner.* **17**, 561-568 (1980).
25. Zabel, M. & Range, K. J. Phase-Relationships in the Tl₂Fe_xS₄ System ($2.6 \leq x \leq 3.6$). *Rev. De Chim. Miner.* **21**, 139-143 (1984)
26. Sabrowsky, H., Rosenberg, M., Welz, D., Deppe, P. & Schafer, W. A neutron and Mössbauer study of TlFe_xS₂ compounds. *J. Magn. Magn. Mater.* **54-57**, 1497-1498 (1986).
27. Haggstrom, L., Seidel, A. & Berger, R. A. Mössbauer Study of Antiferromagnetic Ordering in Iron Deficient TlFe_{2-x}Se₂. *J. Magn. Magn. Mater.*

- 98**, 37-46 (1991).
28. Klingkeler, R. Local antiferromagnetic correlation in the iron pnictide superconductors $\text{LaFeAsO}_{1-x}\text{F}_x$ and $\text{Ca}(\text{Fe},\text{Co})_2\text{As}_2$ as seen via normal-state susceptibility. *Phys. Rev. B* **81**, 024506 (2010)
 29. Wang, X. F. *et al.* Anisotropy in the Electrical Resistivity and Susceptibility of Superconducting BaFe_2As_2 Single Crystals. *Phys. Rev. Lett.* **102**, 117005 (2009).
 30. Yan, J. Q. *et al.* Structural transition and anisotropic properties of single-crystalline SrFe_2As_2 . *Phys. Rev. B* **78**, 024516 (2008).
 31. Wu, G. *et al.* Different resistivity response to spin-density wave and superconductivity at 20 K in $\text{Ca}_{1-x}\text{Na}_x\text{Fe}_2\text{As}_2$. *J.Phys.-Condens. Matter* **20**, 422201 (2008).
 32. Zhang, G. M. *et al.* Universal linear-temperature dependence of the static magnetic susceptibility in iron pnictides, *Europhys. Lett.* **86** 37006(2009)
 33. Yang, J.H. *et al.* Magnetic and superconducting properties in single crystalline $\text{Fe}_{1+\delta}\text{Te}_{1-x}\text{Se}_x$ ($x < 0.5$) system. *J. Phys. Soc. Jpn.* **79**, 074704(2010)
 34. Laad, M. S. & Craco, L. Anomalous magnetic susceptibility in iron pnictides: paramagnetic phase. arXiv: 0903.3732
 35. Johnston, D.C. in Handbook of Magnetic Materials, Vol. 10, edited by Buschow, K. H. J., Ch.1 (Elsevier, Amsterdam, 1997), pp. 1-237
 36. Zhu, J. X. *et al.* Band Narrowing and Mott Localization in Iron Oxychalcogenides $\text{La}_2\text{O}_2\text{Fe}_2\text{O}(\text{SeS})_2$. *Phys. Rev. Lett.* **104**, 216405 (2010)
 37. Zhang, L. & Singh, D. J. Density functional study of the overdoped iron chalcogenide TlFe_2Se_2 with ThCr_2Si_2 structure. *Phys. Rev. B* **79**, 094528 (2009).

Acknowledgements: This work is supported by the Nature Science Foundation of China, the National Basic Research Program of China (973 Program), and PCSIRT of the Ministry of Education of China. We acknowledge Qimiao Si and Jianhui Dai for discussion and encouragement.

Author Contributions: M.H.F. designed this study, analysed the data, did partially the experiments and wrote the paper. H.D.W. did the main experiments and analysed the data. C.H.D., Z.J.L. and C.M.F measured the resistivity and prepared partially samples. J.C. measured partially susceptibility. H.Q.Y provided experimental support.

Author Information: The authors declare that they have no competing financial interests. Correspondence and requests for materials should be addressed to M.H.F (mhfang@zju.edu.cn)

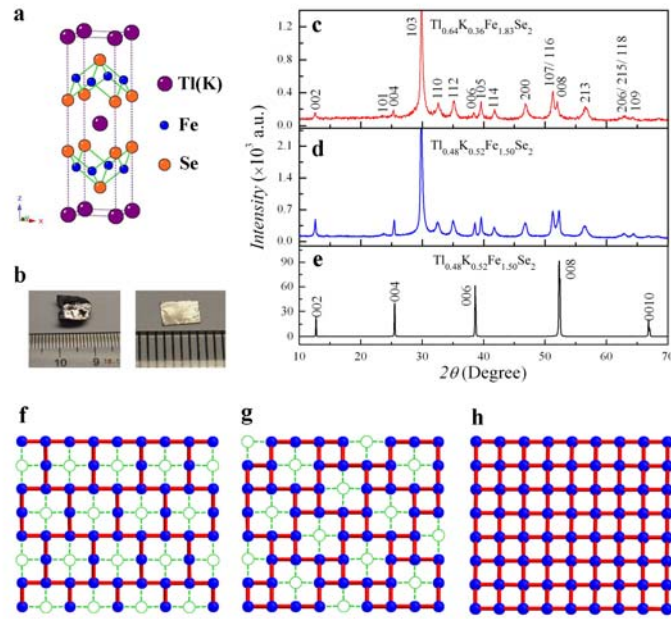


Figure 1 | **Crystal structure and super-lattice of the Fe-vacancy in (Tl,K)Fe_xSe₂.**

a, Crystal structure of stoichiometric $Tl_{1-y}K_yFe_2Se_2$. Tl/K and Se are fully occupied sites of the tetragonal $ThCr_2Si_2$ structure. Fe are partially occupied sites, there are always vacancies partial occupied Fe site due to the requirement of charge-balance as $(Tl,K)^{1+}Fe^{2+}_xSe^{2-}_2$. We found that for $TlFe_xSe_2$ system, $x \leq 1.7$, for $Tl_{1-y}K_yFe_xSe_2$ system ($y \neq 0$), $x \leq 1.88$, which provides a chance to introduce electrons by modifying the Fe content. **b**, Photos of $Tl_{0.48}K_{0.52}Fe_{1.50}Se_2$ crystals before cleaved and one piece crystal of $Tl_{0.64}K_{0.36}Fe_{1.83}Se_2$. **c**, Powder x-ray diffraction (XRD) pattern of $Tl_{0.64}K_{0.36}Fe_{1.83}Se_2$, the powder was obtained by grinding many pieces of crystals. **d**, Powder XRD pattern of $Tl_{0.48}K_{0.52}Fe_{1.50}Se_2$. **e**, Single crystals XRD pattern of $Tl_{0.48}K_{0.52}Fe_{1.50}Se_2$. **f**, Possible Fe-vacancy order of $(Tl,K)Fe_{1.5}Se_2$. Blue solid circle denotes: Fe atom, Green hollow circle denotes: Vacancy. The iron atoms have two or three iron neighbors. **g**, Possible Fe-vacancy order of $(Tl,K)Fe_{1.6}Se_2$, all iron atoms have three identical neighbors. Both patterns were suggested by M. Zabel et al.^{24, 25}, Sabrowsky et al.²⁶ and Haggstrom et al.²⁷ for the explanation of AFM in $TlFe_xSe_2$ and $TlFe_xS_2$ compounds, based on their Mössbauer and neutron diffraction studies. **h**, Fe^{2+} square planar for stoichiometric $(Tl,K)Fe_2Se_2$, which exists in all the Fe-based superconductors. All iron atoms have four iron neighbors. In $(Tl,K)Fe_xSe_2$, the number of iron nearest neighbors varies with composition.

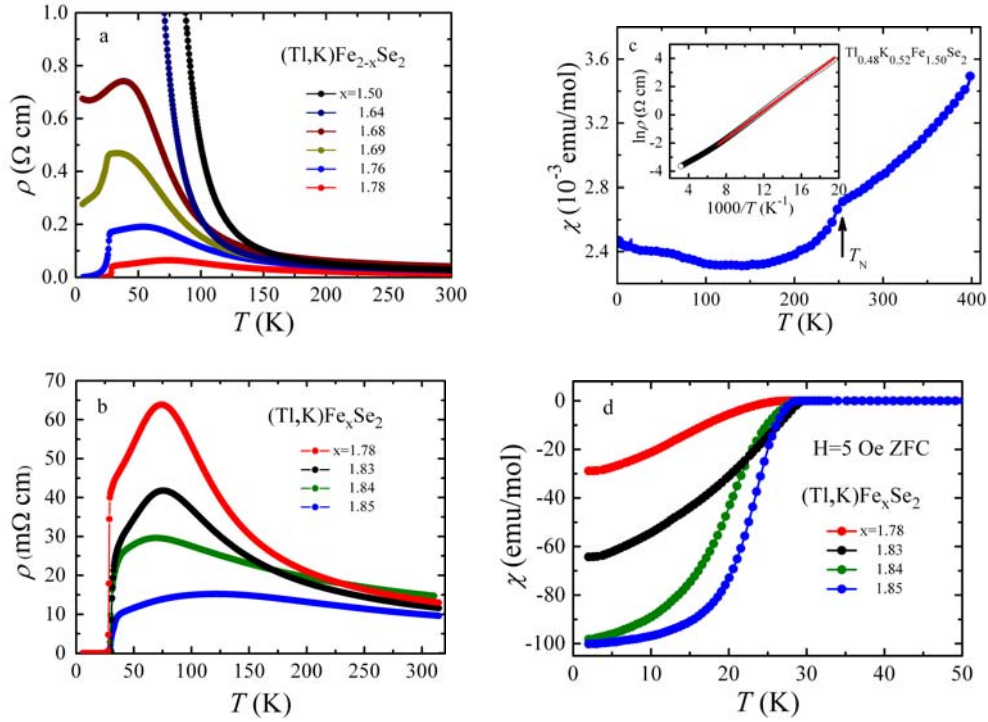


Figure 2 | **Resistivity and Magnetic susceptibility of $(\text{Tl,K})\text{Fe}_x\text{Se}_2$ ($1.50 \leq x \leq 1.85$).** **a**, In-plane resistivity $\rho(T)$ as a function of temperature for $(\text{Tl,K})\text{Fe}_x\text{Se}_2$ ($x=1.50, 1.64, 1.68, 1.69, 1.76$ and 1.78) crystals. **b**, $\rho(T)$ for $(\text{Tl,K})\text{Fe}_x\text{Se}_2$ ($x=1.78, 1.83, 1.84$, and 1.85) crystals. **c**, The temperature dependence of magnetic susceptibility, $\chi(T)$, measured at 1 Tesla magnetic field with field cooling process. The inset is $\ln \rho$ as a function of $1/T$ for $\text{Tl}_{0.48}\text{K}_{0.52}\text{Fe}_{1.50}\text{Se}_2$ crystal. **d**, Magnetic susceptibility data measured with a zero-field cooling history and a field of 5 Oe for $(\text{Tl,K})\text{Fe}_x\text{Se}_2$ ($x=1.78, 1.83, 1.84$ and 1.85) crystals. Both magnetic susceptibility and resistivity show that bulk superconductivity occurs in the crystals with $x \geq 1.78$, and the superconducting volume fraction increases with the increase of x value. The $\chi(T)$ behavior for the $x=1.50$ crystal, which is a thermally-activated semiconductor with an activation energy E_a of 36 meV, is very similar to that in the BaFe_2As_2 , which is a parent of 122-type iron-pnictide and a metal.

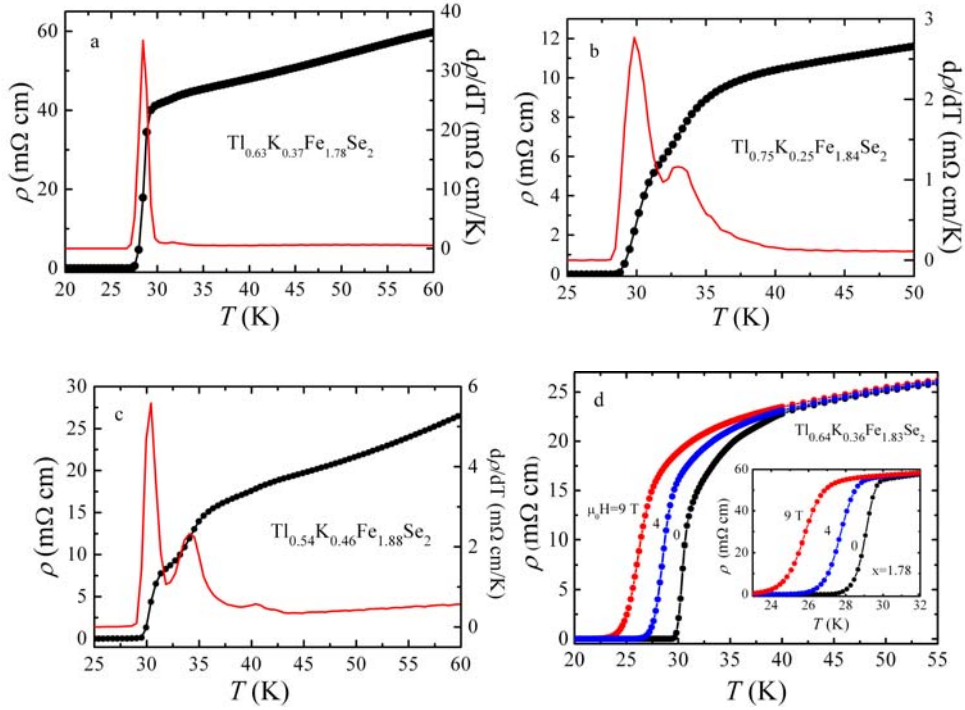


Figure 3 | The superconducting transition of four typical (Tl,K)Fe_{1.78}Se₂ crystals.

a, The temperature dependence of *ab*-plane resistivity, $\rho(T)$, and its differential $d\rho(T)/dT$ near the superconducting transition for Tl_{0.63}K_{0.37}Fe_{1.78}Se₂ crystal. Only one transition appears at $T_c^{\text{mid}}=28.4\text{K}$. **b**, $\rho(T)$ and its differential $d\rho(T)/dT$ for Tl_{0.75}K_{0.25}Fe_{1.84}Se₂ crystal. Two transitions occur at $T_c=29.8\text{K}$ and 33.0K , respectively. **c**, $\rho(T)$ and its differential $d\rho(T)/dT$ for Tl_{0.54}K_{0.46}Fe_{1.88}Se₂ crystal, which is one with the highest Fe content gotten by us. Three transitions occur at $T_c=30.4, 34.1, \text{ and } 40.4\text{K}$, respectively. **d**, $\rho(T)$ near the superconducting transition in magnetic field of 0, 4, and 9 Tesla for Tl_{0.64}K_{0.36}Fe_{1.83}Se₂ crystal, the transition starts at 40K. The inset shows the $\rho(T)$ at 0, 4, and 9 Tesla for Tl_{0.63}K_{0.37}Fe_{1.78}Se₂ crystal, which has only one transition. The multi-transition in $\rho(T)$ was observed in all the crystals with $x \geq 1.83$, regardless of the K content.

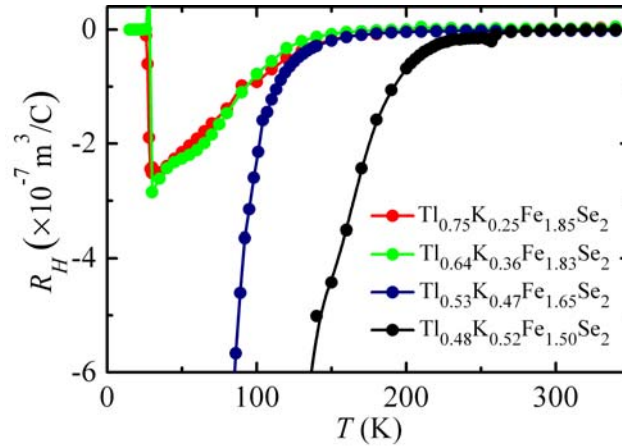


Figure 4 | **The temperature dependence of Hall coefficient, $R_H(T)$, for $(\text{Tl,K})\text{Fe}_x\text{Se}_2$ ($x=1.50, 1.64, 1.83$ and 1.84) crystals.** The negative value of R_H indicates the carriers dominated by electrons in $(\text{Tl,K})\text{Fe}_{2-x}\text{Se}_2$ compound. For both $\text{Tl}_{0.48}\text{K}_{0.52}\text{Fe}_{1.50}\text{Se}_2$ and $\text{Tl}_{0.53}\text{K}_{0.47}\text{Fe}_{1.64}\text{Se}_2$ crystals, the $|R_H|$ value increases sharply at $T_N=250$ and 123K , respectively, indicating that an electron localization occurs at AFM transition temperature. The increase of the Fe-content results in the enhancement of the carrier concentration ($|R_H|$ value decrease), which can be regards as a self-doping of Fe^{2+} electron to the Fe layer with a super-lattice of Fe vacancy. The R_H value seems to be independent of the K content in the crystals.

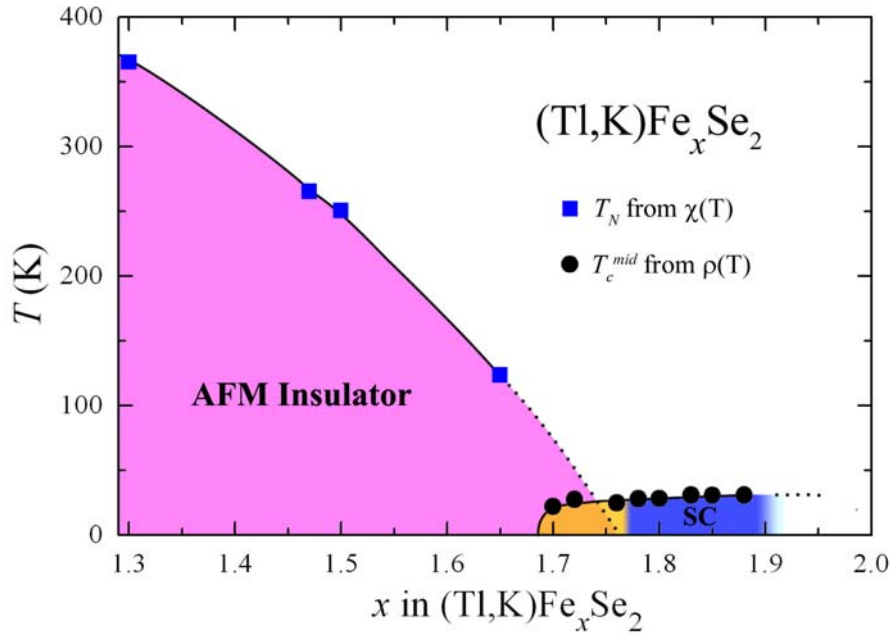


Figure 5 | **The phase diagram of the magnetism and superconductivity for $(\text{Tl,K})\text{Fe}_x\text{Se}_2$ ($1.30 \leq x \leq 1.88$).** The Néel temperature, T_N , of the AFM phase, is determined by the onset temperature of the transition in susceptibility $\chi(T)$. The superconducting transition temperature, T_c^{mid} , is determined by the middle temperature of the transition in $\rho(T)$. In the $1.3 \leq x < 1.7$ region, the compound is an AFM insulator, which may be associated with the existence of various super-lattice of Fe-vacancy. In the region of $1.70 \leq x < 1.78$, a superconducting transition was observed in $\rho(T)$, but superconducting volume fraction is less than 3% estimated from the susceptibility data. An inhomogeneity of Fe-vacancy distribution may result in the coexistence of superconductivity and insulator phase. In the region of $1.78 \leq x \leq 1.88$, bulk superconductivity emerges. The observation of multi-transition in $\rho(T)$ for the crystals with $x \geq 1.83$ implies that phase separation may occur in the crystals. And an optimal Fe content for bulk superconductivity with the highest $T_c=40\text{K}$ is difficult to get in this system due to the limitation of Fe valence.

Supplementary Information:

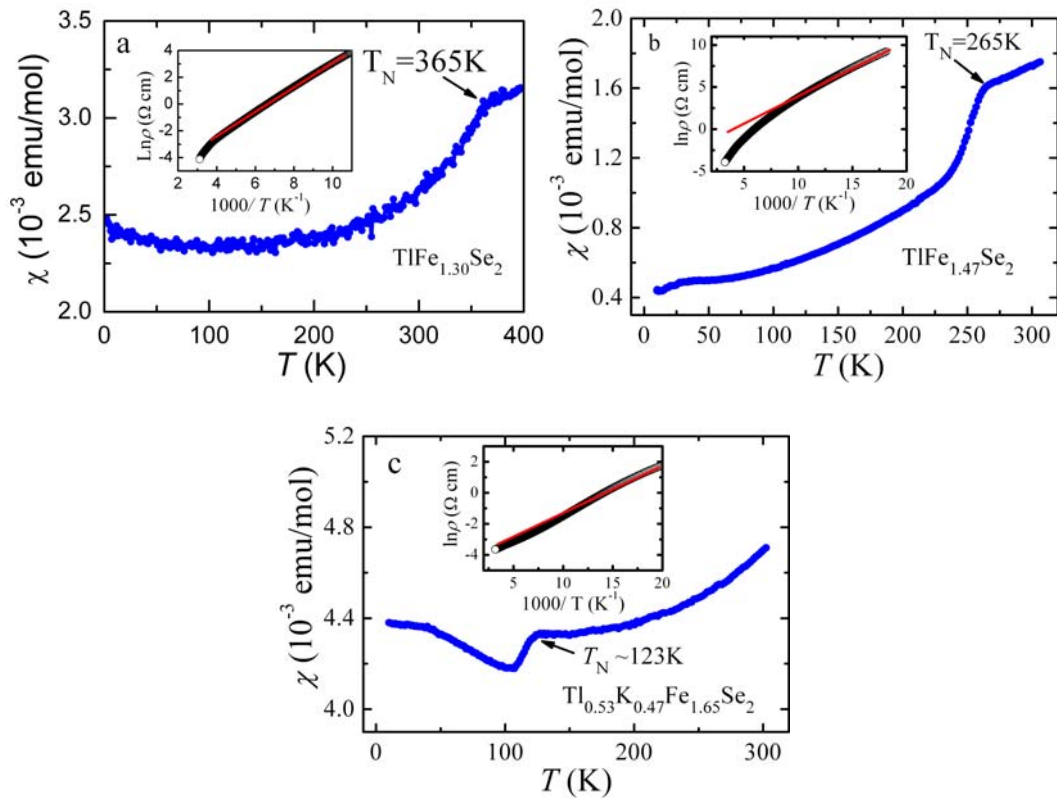


Figure S1| **Temperature dependence of magnetic susceptibility, $\chi(T)$, and $\ln \rho$ as a function of $1/T$ for three insulators. a,** For $\text{TlFe}_{1.30}\text{Se}_2$ crystal. $\chi(T)$, measured at 1 Tesla magnetic field. The inset is the $\ln \rho$ versus $1/T$, an activation energy E_a of 80.2 meV was estimated from the fitting as the red line. **b,** For $\text{TlFe}_{1.47}\text{Se}_2$ crystal. $\chi(T)$, measured at 1 Tesla magnetic field. The inset is the $\ln \rho$ versus $1/T$, an activation energy E_a of 57.7 meV was estimated from the fitting as the red line. **c,** For $\text{Tl}_{0.53}\text{K}_{0.47}\text{Fe}_{1.65}\text{Se}_2$ crystal. $\chi(T)$, measured at 1 Tesla magnetic field. The inset is the $\ln \rho$ versus $1/T$, an activation energy E_a of 24 meV was estimated from the fitting as the red line. At low temperature, χ value shows an upturn, presumably due to small amount impurities in the crystal.

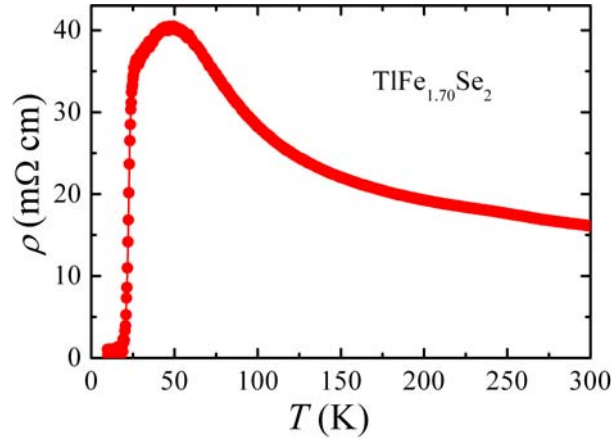


Figure S2 | **The temperature dependence of *ab*-plane resistivity, $\rho(T)$, for $\text{TlFe}_{1.70}\text{Se}_2$ crystal.** Above 50K, $\rho(T)$ exhibits a semiconducting behavior, *i.e.* ρ increases with decreasing temperature. A superconducting transition occurs at $T_c^{\text{onset}}=24.3\text{K}$, $T_c^{\text{mid}}=22.4\text{K}$ and $T_c^{\text{zero}}=20\text{K}$.

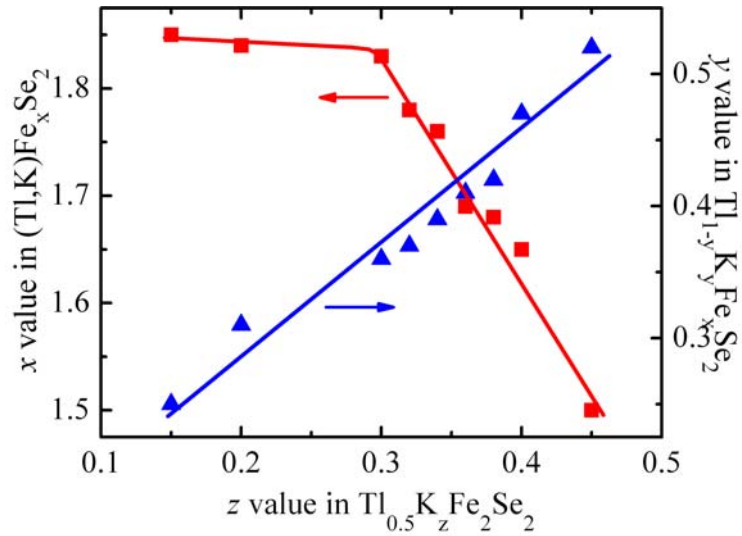


Figure S3 | **The Fe and K contents in the grown crystal as a function of K content, z value, in the starting materials with a nominal composition $\text{Tl}_{0.5}\text{K}_z\text{Fe}_2\text{Se}_2$.** The K content in the grown crystals increases linearly with increasing K content in the starting materials. When $0.3 \leq z \leq 0.45$, the Fe content in the grown crystals increases near linearly with the decreasing of K content in the starting material, and goes almost up to a saturation value of 1.83 at $z=0.3$.

Table S1 | Nominal composition in the starting materials, average composition for the grown crystals determined by EDXS, lattice parameters a and c values for crystals from the fitting XRD data, Neel temperature, T_N , determined by the onset temperature of transition in $\chi(T)$, superconducting transition, T_c^{mid} and T_c^{zero} determined by $\rho(T)$ data.

Nominal composition	Average composition of the grown crystal	a value (Å)	c value (Å)	T_N (K)	T_c^{mid} (K)	T_c^{zero} (K)
TlFe _{1.60} Se _{2.2}	TlFe _{1.30} Se ₂	3.90	13.89	365		
TlFe _{1.50} Se ₂	TlFe _{1.47} Se ₂	3.90	13.95	265		
Tl _{0.80} Fe ₂ Se ₂	TlFe _{1.70} Se ₂				22.4	20.0
Tl _{0.4} K _z Fe ₂ Se ₂						
z=0.20	Tl _{0.69} K _{0.31} Fe _{1.87} Se ₂				31.2	27.9
0.30	Tl _{0.61} K _{0.39} Fe _{1.86} Se ₂				29.2	28.2
0.40	Tl _{0.53} K _{0.47} Fe _{1.80} Se ₂				28.5	27.7
Tl _{0.8-z} K _z Fe ₂ Se ₂						
z=0.10	Tl _{0.86} K _{0.14} Fe _{1.72} Se ₂				27.9	<2K
0.20	Tl _{0.74} K _{0.26} Fe _{1.83} Se ₂				31.2	28.9
0.30	Tl _{0.64} K _{0.36} Fe _{1.83} Se ₂				31.1	30.1
0.40	Tl _{0.53} K _{0.47} Fe _{1.80} Se ₂				28.5	27.7
Tl _{0.3} K _{0.3} Fe ₂ Se ₂	Tl _{0.54} K _{0.46} Fe _{1.88} Se ₂				31.3	29.5
Tl _{0.5} K _z Fe ₂ Se ₂						
z=0.15	Tl _{0.75} K _{0.25} Fe _{1.85} Se ₂	3.88	14.06		31.0	28.8
0.20	Tl _{0.69} K _{0.31} Fe _{1.84} Se ₂	3.88	14.05		30.4	28.9
0.30	Tl _{0.64} K _{0.36} Fe _{1.83} Se ₂	3.87	14.05		29.2	28.2
0.32	Tl _{0.63} K _{0.37} Fe _{1.78} Se ₂				28.4	27.4
0.34	Tl _{0.61} K _{0.39} Fe _{1.76} Se ₂	3.80	14.06		25.1	<2K
0.36	Tl _{0.59} K _{0.41} Fe _{1.69} Se ₂					
0.38	Tl _{0.58} K _{0.42} Fe _{1.68} Se ₂					
0.40	Tl _{0.53} K _{0.47} Fe _{1.65} Se ₂	3.89	14.06	123		
0.45	Tl _{0.48} K _{0.52} Fe _{1.50} Se ₂	3.91	13.99	250		